Universal negative magnetoresistance in antiferromagnetic metals caused by symmetry breaking of electron wave functions

Pavel D. Grigoriev, ^{1,2,3} Nikita S. Pavlov, ^{4,5} Igor A. Nekrasov, ⁴ Igor R. Shein, ⁶ Andrey V. Sadakov, ⁵ Oleg A. Sobolevskiy, ⁵ Evgeny Maltsev, ^{7,8} and Vladimir M. Pudalov ⁵

¹L.D. Landau Institute of Theoretical Physics, RAS, Chernogolovka, 143423, Russia ² National University of Science and Technology "MISiS", 119049, Moscow, Russia ³ HSE University, Moscow 101000, Russia ⁴ Institute for Electrophysics, RAS, Ekaterinburg, 620016, Russia ⁵ V. L. Ginzburg Research Center at P. N. Lebedev Physical Institute, RAS, Moscow 119991, Russia ⁶ Institute of Solid State Chemistry, RAS, Ekaterinburg, 620990, Russia ⁷ Leibniz Institute for Solid State and Materials Research, IFW Dresden, D-01069 Dresden, Germany ⁸ Dresden-Würzburg Cluster of Excellence ct.qmat, Dresden, Germany (Dated: November 19, 2025)

Layered van der Waals crystals of topologically non-trivial and trivial semimetals with antiferromagnetic (AFM) ordering of magnetic sublattice are known to exhibit a negative magnetoresistance that is well correlated with AFM magnetization changes in a magnetic field. This effect is reported in several experimental studies with $EuFe_2As_2$, $EuSn_2As_2$, $EuSn_2P_2$, etc., where the resistance decreases quadratically with field by about 5% up to the spin-polarization field. Although this effect is well documented experimentally, its theoretical explanation is missing up to date. Here, we propose a theoretical mechanism describing the observed magnetoresistance that is inherent in AFM metals and is based on violation the binary \hat{T}_2 symmetry. It is almost isotropic to the field and current directions, contrary to the known mechanisms such as giant magnetoresistance and chiral anomaly. The proposed intrinsic mechanism of magnetoresistance is strong in a wide class of the layered AFM-ordered semimetals. The theoretically calculated magnetoresistance is qualitatively consistent with experimental data for crystals of various composition.

Topology incorporated with magnetism provides a fertile playground for studying novel quantum states and therefore attracts tremendous attention. Topological aspects and related electronic phenomena occuring in antiferromagnetic (AFM) materials are among the central topics in condensed matter physics. Clarifying the underlying mechanisms that govern mutual effects of the magnetic ordering, broken symmetry, exchange and spinorbit coupling on magnetotransport in layered crystals is crucial for comprehending emergent properties and phenomena in spintronics.

The vast majority of layered AFM crystals of topological insulators (TI) and semimetals exhibit such characteristic feature as a negative magnetoresistance (NMR) in external magnetic field. This effect has recently attracted a great deal of interest, as it is related with chiral anomaly in Dirac and Weyl semimetals [1, 2], with Chern insulators and anomalous quantized Hall state in AFM topological insulators [3, 4]. Indeed, for topological semimetals (Na₃Bi, TaS, Cd₃As₂), a large NMR results from the chiral anomaly [5, 6] and appears when electric field is applied nearly parallel to magnetic field. This NMR is highly anisotropic and its sign changes as the angle between the magnetic field H and current increases to $\pi/2$ [5]. In the topological insulator MnBi₂Te₄, a huge NMR [4] occurs as a result of the topological phase transition from AFM TI to a ferromagnetic Weyl semimetal in external field.

On the other hand, a number of layered crystals of topologically trivial AFM semimetals ($EuSn_2As_2$ [7–9], $EuSn_2P_2$ [10], $CaCo_2As_2$ [11], $CsCo_2Se_2$ [12], etc.) ex-

hibit isotropic negative magnetoresistance (NIMR) for transport both along and across the layers. There is no satisfactory treatment of such isotropic NMR. Particularly, the magnetoresistance (MR) related with magnon scattering is negative only in ferromagnets and arises from the magnetic-field-induced suppression of scattering [13]. For antiferromagnets, the magnon scattering causes positive MR [14, 15] [16] that originates from a field-induced increase in spin fluctuations.

Negative giant MR (GMR) is well known for the Fe/Cr superlattices where resistance decreases as magnetization in the neighbouring Fe-layers turns with external magnetic field from antiparallel to parallel [17, 18]. For ideal interfaces, GMR should develop for charge transport across the layers [18]. In experiments with artificially deposited Fe/Cr layers [17], a weaker NMR is observed also for current along the layers and is associated with diffuse scattering at layer boundaries [19, 20]. Another case, the "colossal" NMR is known for doped manganites and magnetic granular samples [18, 20, 21] where domains due to phase separation effects and misoriented crystallites lead to electron scattering at the boundaries.

In case of high quality *single crystals*, the scattering by grains, domain or crystallite boundaries is missing; also, there is not much sense to consider roughness of atomic layers. The isotropy of experimentally observed NIMR encourages us to consider scattering by point defects.

In this paper we suggest a mechanism of the *intrinsic* isotropic NMR that is irrelevant to magnons, magnetic impurities, grain boundaries, layer roughness, and topology, being general to AFM metals and rather strong in

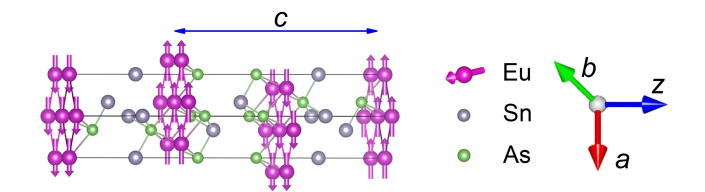


FIG. 1. Schematic picture of the EuSn₂As₂ lattice structure (adapted from Ref. [24]). Magenta arrows show Eu-atoms magnetization direction in the A-type AFM ordered state. For more detail on the Eu magnetic moments orientation, see Supplementary Note 3. Horizontal arrow denotes the lattice spacing $c \approx 2.64$ nm along z-axis [7, 8, 25].

a wide class of the anisotropic layered crystals of AFM metals and semimetals. These materials exhibit a negative magnetoresistance that is tightly correlated with the magnetization field dependence [8–10, 22, 23]. The magnetization changes linearly with external field and sharply saturates above a field of complete spin polarization $H_{\rm sf}$ (see **Supplementary Note 1**); the $H_{\rm sf}$ field is often called spin-flip field for the easy axis case. Though the close relationship between magnetization and magnetoresistance is known also for GMR and colossal MR (CMR) [18, 21], the suggested mechanism is completely different.

We test our model by comparing it with experimentally measured magnetoresistance in EuSn₂As₂ that has a topologically trivial BS (see **Supplementary Note 2**). For this representative compound, at T < 24 K the magnetic Eu-sublattice experiences magnetic ordering into the A-type AFM structure where Eu magnetic moments lie in the easy ab-plane and rotate by π from layer to layer along the z-axis (see Fig. 1a, and also **Suplementary Note 3**).

Synchronous with magnetization, the diagonal resistivity decreases approximately parabolically with field as $\delta \rho_{xx}(H) \propto -\alpha H^2$. At higher fields $H > H_{\rm sf}$, magnetotransport perpendicular to the field sharply changes from NMR to a conventional positive magnetoresistance. Such NMR in layered AFM crystals, closely correlated with the field dependence of magnetization M(H) [8–10, 22], was discussed previously in terms of either nontrivial topological properties, or in terms of scattering by domains, grain boundaries etc., with no detailed theoretical consideration.

In this paper we address the issue of the origin of negative isotropic MR. Specifically, we (i) propose a model where NIMR universally originates from the enhancement of electron scattering in AFM crystals, (ii) substantiate this proposal using the density functional theory (DFT) calculations of spin polarized charge distribution, and (iii) compare the model quantitatively with our experimental data for NIMR in EuSn₂As₂ and qualitatively – with other compounds of the same class of layered AFM crystals.

Results

Model and a qualitative consideration

The main idea of the proposed NIMR mechanism is as follows. The AFM order violates the binary \hat{T}_2 symmetry $1\leftrightarrow 2$ between two magnetic sublattices (adjacent layers in EuSn₂As₂, see Fig. 1). This \hat{T}_2 symmetry to the permutation of AFM sublattices is irrelevant to topology and means equal energies and weights of electron eigenfunctions on each AFM sublattice. Its violation leads to spatial redistribution of wave functions (WF) $\psi_{\sigma}(r)$ for two different spin projections ($\sigma = \uparrow \downarrow$) and to their concentration near the corresponding AFM sublattices. As a result of this WF squeezing, the electron scattering rate [26] by short-range crystal defects or δ -correlated disorder increases already in the Born approximation:

$$1/\tau \propto \int |\psi_{\sigma}(\mathbf{r})|^4 d^3 \mathbf{r}. \tag{1}$$

Figure 2 schematically illustrates this \hat{T}_2 -symmetry violation of electron eigenfunctions by AFM order and the resulting enhancement of $|\psi_{\sigma}|^4(r)$ entering the scattering rate in Eq. (1).

As we show below in Eqs. (6) and (11), the degree of \hat{T}_2 symmetry violation, given by Eq. (6), and the corresponding $1/\tau$ enhancement, given by Eq. (11), depend on the ratio $\gamma = E_{ex}/2t_0$ of the exchange splitting E_{ex} of conduction electron bands to their hopping amplitude t_0 between the opposite AFM sublattices (Fig. 1). In the main order in γ this relative enhancement of $1/\tau$ is

$$-\delta\tau/\tau \approx \gamma^2 = (E_{ex}/2t_0)^2. \tag{2}$$

While t_0 is determined by the band structure and does not considerably depend on magnetic field H, the exchange splitting $E_{ex} \propto L_{AFM}(H)$ decreases with H according to the mean-field theory (see, e.g. Eq. (3) of Ref. [27] and Eq. (24) of Ref. [28]):

$$\frac{E_{ex}(H)}{E_{ex}(H=0)} = \frac{L_{AFM}(H)}{L_{AFM}(0)} \approx \sqrt{1 - \left(\frac{H}{H_{\rm sf}}\right)^2}.$$
 (3)

Here L_{AFM} is the AFM order parameter, i.e. the difference of magnetization $M_{1,2}$ of two AFM sublattices: $L_{AFM} = M_1 - M_2$. Eq. (3) can be derived as follows. In a sufficiently large field $H \leq H_{\rm sf}$, the AFM order parameter $L_{AFM} \perp H$ [29]. In this range the field also causes a net magnetization $M = M_1 + M_2 = \chi H$, coming mainly from the nonzero averaged spins $\langle S \rangle$ of magnetic atoms, Eu in our case. The corresponding magnetic susceptibility χ is approximately constant as a function of field at temperature $T < T_N$ below the Neel temperature T_N [29]: $\chi(H) \approx const.$ This is also confirmed by direct AC susceptibility and DC magnetization [30] in a field $H \leq H_{\rm sf}$. The total spin of each magnetic ion is fixed, $S_{||}^2 + S_{\perp}^2 = \hat{S}^2 = S(S+1)$, where $S_{||}$ and S_{\perp} are its components parallel and perpendicular to magnetic field, giving the net magnetization M and AFM order parameter

 ${\cal L}_{AFM}$ correspondingly. Then $L_{AFM}/M = \langle S_{\perp} \rangle / \langle S_{||} \rangle$ leads to

$$\boldsymbol{L}_{AEM}^2 + \boldsymbol{M}^2 = \boldsymbol{L}_{AEM}^2 + (\chi \boldsymbol{H})^2 = const \qquad (4)$$

and to the right side of Eq. (3).

For our model of negative magnetoresistance, we only need the exchange interaction between the magnetic ions (or even their sublattices) and conduction electrons. It is nearly a point-like Heisenberg interaction $-\mathcal{J}S\sigma$ between the spin S of magnetic ion and the spin $\sigma/2$ of conduction electrons, because the exchange coupling is strong only where the wave functions of conduction electrons overlap with the localized electrons of magnetic ions. The wave function $\psi_{\sigma}(r)$ of conduction electron is delocalized and extended to many magnetic ions. Therefore, $\psi_{\sigma}(r)$ feels an average spin $\langle S_i \rangle$ of magnetic ions on each AFM sublattice i, which is proportional to its total magnetization M_i . Hence, instead of considering the interaction between individual Eu atoms and electrons, we only need the mean-field average spin $\langle S_i \rangle \propto M_i$, which creates a spin-dependent potential for conduction electrons.

The spin S of magnetic atoms is only reoriented by magnetic field, leaving $L_{AFM} \perp H$ over the intire range $H < H_{sf}$. Hence, the absolute value S = |S| of spin moment and of the exchange-splitting of conducting electrons is independent of magnetic field. This splitting from electron exchange interaction is usually calculated using the DFT in collinear form, especially for Eu with half-filled 4f orbitals carrying a local moment. We denote this splitting $E_{ex0} = E_{ex}(H=0)$ in Eq. (3); below from our DFT calculations we estimate it to be $E_{ex0} \approx 30 \text{meV}$ for EuSn₂As₂. The exchange splitting $E_{ex} = E_{ex}(H)$, entering our NIMR mechanism and Eqs. (2)-(3), is the difference of exchange energy on two different AFM sublattices. The AFM order parameter L_{AFM} also gives the difference between averaged spin orientation of magnetic atoms on these two AFM sublattices, which determines the exchange splitting $E_{ex} = E_{ex}(H)$. Hence, $L_{AFM}(H) \propto E_{ex}(H)$, as we write in the left part of Eq. (3).

Indeed, for the NIMR effect, coming from the redistribution of $\psi_{\sigma}(r)$ between two AFM sublattices as given by Eq. (6) below, we need the difference of weights of $\psi_{\sigma}(r)$ on two different AFM sublattices. And this difference of weights is proportional to the difference E_{ex} , entering the Hamiltonian in Eq. (5), of the averaged exchange energy $J\langle S_i\rangle$ of conducting electrons on two different AFM sublattices. Since $J\langle S_i\rangle \propto M_i$, we get $E_{ex} = -\mathcal{J}(S_1 - S_2) \propto -\mathcal{J}(M_1 - M_2) = -\mathcal{J}L_{AFM}$. This gives the left-side part of Eq. (3). This analysis also shows that the low index σ in the wave function $\psi_{\sigma}(r)$ is the projection of conducting-electron spin on the AFM order parameter L_{AFM} .

Eqs. (2) and (3) lead to a parabolic isotropic negative magnetoresistance (NIMR) persisting almost up to the spin polarization field $H_{\rm sf}$.

Quantitative consideration

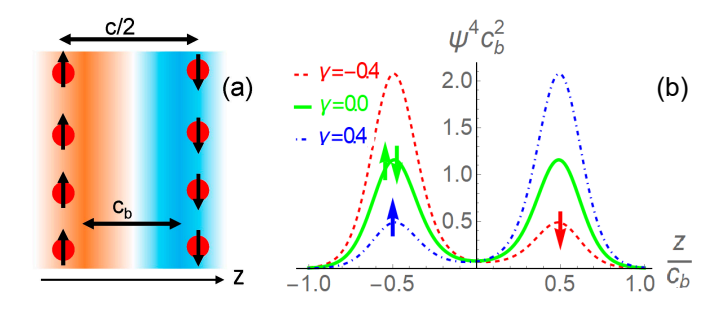


FIG. 2. Wave function (WF) magnitude distribution along the crystal z-axis for the lowest-energy quantum state [Eq. (6)] in a double-well potential, modeling two AFM sublattices. a Schematic color illustration of the spin-up (red) and spin-down (blue) wave function distribution along the z-axis in the half-cell of the c/2-size. c_b denotes the distance between the two spin-split WF maxima. Color intensity represents the WF magnitude. Red circles show Eu atoms, and arrows – their magnetization direction in the AFM state. b Schematic picture of the fourth power $\psi^4(z)$ of electron WF given by Eq. (6), entering the scattering rate in Eq. (1). The asymmetry parameter $\gamma \equiv E_{ex}/2t_0 = 0$ (green solid line), $\gamma = -0.4$ (dashed red line) and $\gamma = 0.4$ (dash-dotted blue line).

Let us consider quantitatively the electron WF squeezing in the AFM state. The two AFM sublattices are numerated by the index j = 1, 2, and the spin projection on the AFM magnetization axis L_{AFM} is indexed by $\sigma =$ $\pm 1 \equiv \uparrow, \downarrow$. For each quasi-momentum the quantum basis consists of four states, $|j,\sigma\rangle = \{1\uparrow,1\downarrow,2\uparrow,2\downarrow\}$, corresponding to wave functions $\psi_{j,\sigma} = \{\psi_{1\uparrow}, \psi_{1\downarrow}, \psi_{2\uparrow}, \psi_{2\downarrow}\}.$ The usual Zeeman splitting $E_Z(\mathbf{H}) = (\vec{\sigma} \cdot \vec{\mathbf{H}}) g\mu_B/2$ in a relevant external magnetic field $H \lesssim 5 \text{T}$ is much smaller than the exchange splitting $E_{ex0} \sim 30 \text{meV}$ and is neglected below. The neglected spin-orbit coupling $E_{SOC} \lesssim 5 \text{meV}$ (see Supplementary materials, Note 4) is also much smaller than the exchange splitting E_{ex0} and, additionally, averages to zero after the integration over electron momentum in the first order of perturbation theory. Then for each electron quasi-momentum kthe AFM-sublattice part of electron Hamiltonian is given by the 4×4 matrix, which decouples into two 2×2 matrices:

$$\hat{H}_{\sigma} = \begin{pmatrix} E_{ex}\sigma/2 & t_0 \\ t_0^* & -E_{ex}\sigma/2 \end{pmatrix}. \tag{5}$$

Here the diagonal terms are the energy shifts due to the exchange interaction with AFM magnetization, and the off-diagonal term $t_0 = t_0^*$, the intersublattice electron transfer integral, determines the electron hopping rate between AFM sublattices. The diagonalization of Hamiltonian (5) gives two eigenvalues $\varepsilon_{\pm,\sigma} = \mp \sqrt{E_{ex}^2/4 + t_0^2}$

and the corresponding normalized wave functions

$$\psi_{\pm,\sigma} = \frac{\psi_1 \left(\sigma \gamma \pm \sqrt{\gamma^2 + 1}\right) + \psi_2}{\sqrt{1 + \left(\sigma \gamma \pm \sqrt{\gamma^2 + 1}\right)^2}},\tag{6}$$

where $\psi_{1,2}$ are the electron wave functions "localized" mostly on the first and second AFM sublattices. Without the AFM order, i.e. at $\gamma \propto E_{ex} = 0$, this gives the simple electron spectrum $\varepsilon^0_{\pm,\sigma} = \mp t_0$ and eigenstates $\psi^0_{\pm,\sigma} = (\psi_2 \pm \psi_1)/\sqrt{2} = \psi^0_{\pm}$, which are the symmetric and antisymmetric superpositions of electron states on sublattices 1 and 2 with equal WF weights on each AFM sublattice. From Eq. (6) we see that the AFM order lifts this symmetry, making the eigenfunction amplitude larger at one of the two sublattices at $\gamma \neq 0$ (see Fig. 2). This enhances the electron scattering rate in Eq. (1), as seen from Fig. 2 and estimated below.

In the Born approximation, i.e. the second-order perturbation theory in the impurity potential, the electron scattering rate is given by the Fermi's golden rule [26]:

$$\frac{1}{\tau_{n}} = \frac{2\pi}{\hbar} \sum_{n',i} \left| T_{n'n}^{(i)} \right|^{2} \delta \left(\varepsilon_{n} - \varepsilon_{n'} \right), \tag{7}$$

where the index $\mathbf{n} \equiv \{\mathbf{k}, \beta, \zeta, \sigma\}$ numerates quantum states, β numerates electron bands at the Fermi level coming from different atomic orbitals in multiband metal, $\zeta = \pm$ denotes two eigenstates in Eq. (6), i numerates impurities, ε_n is the electron energy in state n, and $\delta(x)$ is the Dirac delta-function. The additional index $\zeta = \pm$ doubles the number of quantum states per each quasimomentum \mathbf{k} , which compensates the folding in half of the first Brillouin zone by the commensurate AFM.

The short-range impurities or other crystal defects in solids are usually approximated by the point-like potential $V_i(\mathbf{r}) = U\delta(\mathbf{r} - \mathbf{r}_i)$. Here we omit the spin index σ because it is conserved by the potential scattering. The corresponding matrix element of electron scattering is $T_{\boldsymbol{n}'\boldsymbol{n}}^{(i)} = U\Psi_{\boldsymbol{n}'}^*(\boldsymbol{r}_i)\Psi_{\boldsymbol{n}}(\boldsymbol{r}_i)$, where $\Psi_{\boldsymbol{n}}(\boldsymbol{r}) = \psi_{\beta\zeta\sigma}(\boldsymbol{r})\exp\left(i\boldsymbol{k}\boldsymbol{r}\right)$ is the electron Bloch wave function with periodic $\psi_{\beta\zeta\sigma}(\mathbf{r})$. For point-like potential the matrix element $T_{n'n}^{(i)}$ does not depend on electron momentum k'. Then the summation over k' with the δ -function in Eq. (7) gives the electron density of states (DoS) $\nu_{F\beta\zeta\sigma} \equiv \nu_{\beta\zeta\sigma}(\varepsilon_F)$ at the Fermi energy ε_F per one spin component σ and per one subband. The total DoS per one spin $\nu_F = \sum_{\beta\zeta} \nu_{F\beta\zeta\sigma}$ does not depend on σ because the total time-reversal symmetry is conserved by AFM, as the simultaneous change of spin index $\sigma = \pm 1$ and of AFM sublattice $1 \leftrightarrow 2$ (layer in our case) does not change the system. If the impurities are uniformly and randomly distributed in space, the sum over impurities rewrites as an integral over impurity coordinate [26]: $\sum_{i} \rightarrow n_{\text{imp}} \int d^{3} \mathbf{r}_{i}$, where n_{imp} is the impurity concentration. Then Eq. (7) becomes

$$\frac{1}{\tau_n} = \frac{2\pi}{\hbar} n_{\rm imp} U^2 \nu_F I, \tag{8}$$

where the integral over one elementary cell

$$I \equiv \int d^3 \mathbf{r} \left| \psi_{\beta\zeta\sigma} \left(\mathbf{r} \right) \right|^2 \sum_{\beta'\zeta'} \frac{\nu_{F\beta'\zeta'\sigma}}{\nu_F} \left| \psi_{\beta'\zeta'\sigma} \left(\mathbf{r} \right) \right|^2. \tag{9}$$

According to Eq. (6), for each band β the WFs of two opposite subbands $\zeta = \pm$ shift toward opposite AFM sublattices. These states are separated by large energy

$$\Delta \varepsilon_{\zeta} = \varepsilon_{-} - \varepsilon_{+} = 2\sqrt{E_{ex}^{2}/4 + t_{0}^{2}} > 2t_{0}. \tag{10}$$

Hence, rather commonly a single subband ζ appears at the Fermi level, i.e. $\nu_{F\beta\zeta'\sigma}=0$ for $\zeta'\neq\zeta$. Then Eqs. (8),(9) confirm Eq. (1). In fact, it holds even if there are several conducting bands β but only one subband ζ is occupied, because the WF in Eq. (6) does not considerably depend on the band β and enters in the fourth power in Eq. (9). Eqs. (8),(9) approximately give Eq. (1) even when there are several subbands $\zeta=\pm$ on the Fermi level, but their DoS $\nu_{F\beta\zeta\sigma}$ differ strongly. The latter happens in Dirac semimetals, where the DoS $\nu_{\beta\zeta}(\varepsilon_F) \propto \varepsilon_F^{d-1}$ strongly depends on energy ε_F and where the subband splitting $\Delta\varepsilon_{\zeta} \gtrsim \varepsilon_F$.

For the reason explained above, we now consider the case of only one subband $\zeta=+$ at the Fermi level and estimate the difference δI of two integrals (9) with and without AFM, i.e. for $\gamma\neq 0$ and $\gamma=0$. The host crystal lattice has the \hat{T}_2 symmetry, therefore $\int \psi_1^4(z)\,dz=\int \psi_2^4(z)\,dz$. For simplicity, we also assume that the overlap of the wave functions on different AFM sublattices is negligible, i.e. $\psi_1\psi_2\ll |\psi_1|^2$, and we neglect the product $\psi_1\psi_2\approx 0$. The main conclusion remains valid also when $\psi_1\psi_2\sim |\psi_1|^2$, but the calculations are more cumbersome.

Without AFM order, substituting Eq. (6) at $\gamma = 0$ to the integral (9), we obtain $I_0 = \int d^3 \mathbf{r} \left| \psi_+^0 \right|^4 dz \approx \int d^3 \mathbf{r} \left| \psi_+^0 \right|^4 - \left| \psi_+^0 \right|^4$ determines the correction to electron mean free time τ according to Eqs. (1) or (8) and, hence, the NIMR effect. After substituting Eq. (6) at $\psi_1 \psi_2 \ll \left| \psi_1 \right|^2$ it reduces to

$$\delta I \approx \frac{\gamma^2}{1+\gamma^2} \int d^3 \mathbf{r} \frac{\psi_1^4(z)}{2} = \frac{\gamma^2 I_0}{1+\gamma^2} = \frac{\gamma^2 I}{1+2\gamma^2}.$$
 (11)

At $\gamma^2 \ll 1$ Eq. (11) simplifies to $\delta I \approx \gamma^2 I_0 \approx \gamma^2 I$, and substituting Eqs. (11) and (3) to (8) we obtain the relative increase of resistivity due to the AFM ordering

$$\frac{\delta\rho(H)}{\rho(0)} = \frac{\delta I}{I} = \frac{\gamma^2}{1 + 2\gamma^2} \approx \left(\frac{E_{ex0}}{2t_0}\right)^2 \left(1 - \frac{H^2}{H_{sf}^2}\right).$$
 (12)

Contrary to the NMR caused by chiral anomaly in Weyl semimetals and to the GMR in layered heterostructures, this increase of resistivity is *isotropic*. Therefore, our NIMR mechanism applies both for the interlayer and intralayer transport in layered conductors, and only slightly depends on the magnetic field direction due to a

magnetic anisotropy solely.

Classical positive magnetoresistance

At $H > H_{\rm sf}$ the obtained NIMR correction (12) disappears, and for the current J perpendicular to magnetic field direction one returns to the usual classical positive magnetoresistance (CPMR) in multiband conductors due to impurity scattering, which is parabolic at low field when $\omega_c \tau \ll 1$ [25]:

$$\rho_{zz}^{m}\left(H\right)/\rho_{zz}^{m}\left(0\right)\approx1+\omega_{c}^{2}\tau^{2},\ \omega_{c}\tau\ll1,\tag{13}$$

where $\omega_c = eH/(m^*c)$ is the cyclotron frequency and τ - the scattering time for the dominant band [25].

Combining Eqs. (12) and (13) gives the schematic MR curve illustrated in Fig. 3a, which resembles very much typical experimental data measured with the representative compound ${\rm EuSn_2As_2}$ (see Fig. 4a). The sharp transition from negative to positive magnetoresistance at $H=H_{\rm sf}$ happens because our NIMR effect, which is stronger than the classical positive magnetoresistance in A-type AFM layered metals, exists only in the AFM state at $H < H_{\rm sf}$.

It is worth of noting, the simplified model, Eq. (12), is the lowest order theory. Closer to the spin polarization transition, at $H \to H_{\rm sf}$, higher-order magnetization fluctuation effects may cause a faster decrease of $L_{AFM}\left(H\right)$ than that given by Eq. (3).

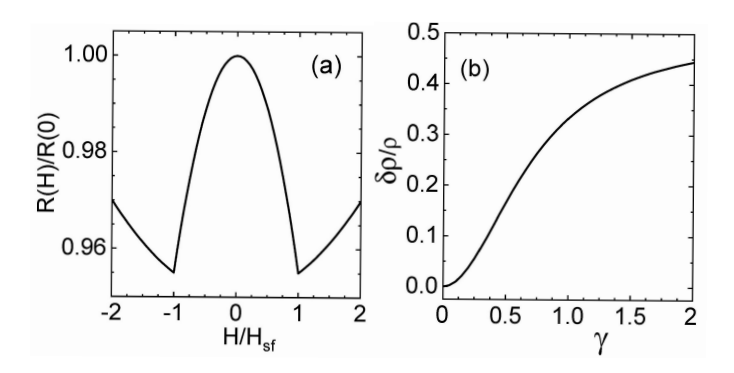


FIG. 3. Calculated negative magnetoresistance. a Magnetoresistance curve given by Eqs. (12) and (13) at $E_{ex0}/2t_z=0.23$ and $[\omega_c\tau(H=H_{\rm sf})]^2=0.2$. b The maximal possible relative value of the proposed NIMR effect as a function of $\gamma_0=E_{ex0}/2t_0$, plotted using Eqs. (11) or (12). It saturates at 50% for $\gamma_0\gg 1$, when resistivity drops by half.

Comparison of the model with experimental data

In isotropic 3D AFM metals, the proposed NIMR mechanism is usually very weak, because the ratio $\gamma = E_{ex}/2t_0 \ll 1$. Indeed, $E_{ex} \lesssim 0.1 \text{eV}$, while $2t_0 \sim 1 \text{eV}$ is comparable to the bandwidth. However, in strongly anisotropic layered AFM semimetals the ratio $\gamma = E_{ex}/2t_0 \sim 1$, because the interlayer transfer integral $t_0 \lesssim 0.1 \text{eV}$ in van-der-Waals or other layered compounds is also small.

To compare the presented theory with experimental data, we performed magnetization and magnetoresistance measurements with EuSn₂As₂ bulk single crystals.

The normalized R(H)/R(0) magnetoresistance and magnetization M(H) dependences are shown in Figs. 4 for various field and current directions, $H\|c$, $H\|(ab)$, $J\|c$, $J\|(ab)$, at our lowest temperature $T\approx 2\,\mathrm{K}\ll T_N\approx 24\,\mathrm{K}$. More detailed magnetization data for various temperatures are presented in Fig. S1 of Supplementary Note 1.

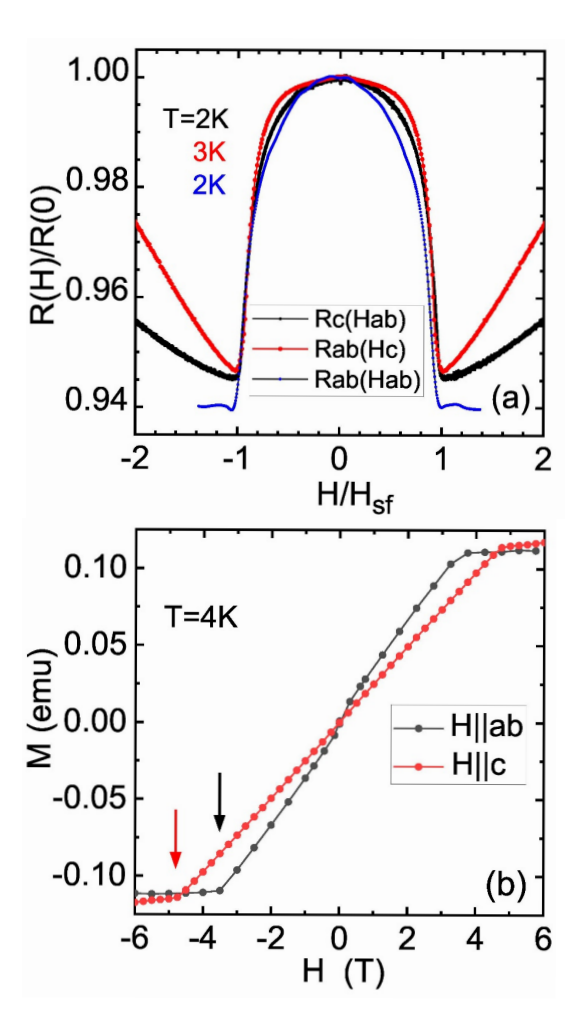


FIG. 4. Experimental data on magnetoresistance and magnetization of $\operatorname{EuSn_2As_2}$ bulk crystal. a Examples of the normalized magnetoresistance R(H)/R(0)) vs normalized field (H/H_{sf}) for two orientations of the bias current, in-plane R_{ab} and perpendicular to the plane R_c , and for two magnetic field directions, $H\|(ab)$ and $H\|c$. Data are taken at T=2-3K. b Magnetization M(H) dependences for two field orientations, $H\|ab$ and $H\|c$. The nonlinearity of $M(H\|ab)$ in low fields is related with spin canting and spin-flop [25]. Vertical arrows depict H_{sf} value for two field orientations.

As field exceeds $H_{\rm sf}$, the NIMR hump changes sharply to the conventional smooth parabolic rise. The sharp transition between the negative and positive magnetoresistance (i.e. the R(H) minimum) coincides with the sharp magnetization saturation at $H = H_{\rm sf}$ for both field directions (Figs. 4a,b), consistent also with previous studies [8, 9, 24, 30, 31]. Comparing this data with the presented first-order in $(\omega_c \tau)^2$ model, we conclude that the model correctly captures the main features: approximately parabolic NMR, its magnitude, and a sharp transition to the conventional CPMR. One can also see in Fig. 4a that CPMR is much weaker for J perpendicular to the layers, than along the ab plane, and is almost missing for $J \parallel H$. This observation is in a qualitative agreement with the simple treatment of CPMR, Eq. (13), and with zero-field conduction anisotropy in van der Waals (vdW)-type layered crystal [25]. The observed NIMR is larger for $J \parallel H$ than for $J \perp H$ just by the magnitude of this CPMR.

The measured NIMR (see Fig. 4a and also refs. [10–12]) looks somewhat more flat than the parabolic dependence (Eq. 12 and Fig. 3a). We presume that flattening of the data in low fields may be caused by magnon scattering that in AFM state results in a positive MR [14, 15]. This scattering mechanism is beyond the framework of our first order theory.

In our measurements on EuSn₂As₂ crystals, the magnetoresistance $\delta \rho/\rho$ drops by about 5 – 6%, as shown in Fig. 4. According to Eq. (12) this drop corresponds to

$$\gamma_0 = E_{ex0}/2t_0 = \sqrt{\delta\rho/\rho} \approx 0.23. \tag{14}$$

We now compare this ratio with our DFT calculations and ARPES data for E_{ex0} and $4t_0$. From the DFT calculations we found $E_{ex0} \approx 30\,\mathrm{meV}$ level splitting for EuSn₂As₂ [25]. Substituting this to Eq. (14) one gets $t_0 \approx 65\,\mathrm{meV}$. The ARPES data [25, 32] do not have sufficient energy resolution to measure the bilayer splitting and t_0 directly. However, the t_0 value can also be roughly estimated from the observed resistivity anisotropy $\rho_{zz}/\rho_{xx} \approx 130$ [25] and the width of the inplane energy band $4t_x \approx 1.9\,\mathrm{eV}$, which is taken from the ARPES data and from the DFT calculation. As a result, we obtain the lowest estimate $t_0 \approx t_x/\sqrt{\rho_{xx}/\rho_{zz}} \approx 42\,\mathrm{meV}$, which is in a reasonable agreement with $t_0 \approx 65\,\mathrm{meV}$ determined from Eq. (14).

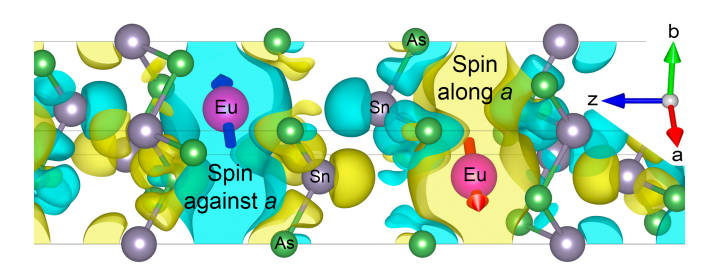


FIG. 5. Calculated spin-polarized electron density distribution. The yellow (turquoise) isosurfaces correspond to fixed differences of charge density with spin along (against) the a axis of AFM ordering of Eu spins. The neighboring SnAs layers have opposite spin polarization of electrons at the Fermi level thus substantiating our model.

Discussion

Now we check whether our assumption of complete ζ -subband polarization is valid for EuSn₂As₂. According to the DFT calculations [25], in EuSn₂As₂ there are two electron bands with $\varepsilon_F \approx 55$ meV and $\varepsilon_F \approx 100$ meV and two hole bands with $\varepsilon_F \approx 65$ meV and $\varepsilon_F \approx 80$ meV. Substituting $t_0 \approx 50$ meV and $E_{ex0} \approx 30$ meV to Eq. (10) we get the ζ -subband splitting $\Delta \varepsilon_\zeta \gtrsim 100$ meV> ε_F for all Fermi-surface pockets. Hence, in EuSn₂As₂ all electronic bands at the Fermi level are completely subband-polarized, and the above analysis of the NIMR effect is applicable to the experimental data in EuSn₂As₂.

In order to substantiate our model of opposite spin polarization of conducting electrons on neighboring SnAs layers, we performed the ab-initio DFT calculation of spin-polarized electron density distribution. Our results are shown in Fig. 5, where the yellow (turquoise) isosurfaces limit the real-space areas filled with the same color of positive (negative) electron spin density exceeding a fixed absolute value. As we assumed in our model and illustrated in Fig. 2, the neighboring SnAs layers indeed have opposite spin polarization of conducting electrons. This spin polarization in EuSn₂As₂ is small, $\sim 0.1\%$ of total electron density, but it is peaked at the Fermi level and strongly affects the electron scattering rate according to the above analysis.

The spin-orbit coupling (SOC) is ignored in our model because the corresponding term E_{SOC} in electron energy is usually much smaller than the exchange coupling E_{ex0} . A weak spin-orbit coupling gives a perturbative correction to the predicted NIMR effect, which is small by the parameter $E_{SOC}/E_{ex0} \ll 1$ and does not affect our NIMR mechanism considerably. Moreover, the spinorbit term in the Hamiltonian is averaged over electron momenta to almost zero in the first order of perturbation theory and affects only in its next orders. Hence, even at $E_{SOC}/E_{ex0} \sim 1$ our NIMR mechanism survives, because it gives the effect averaged over all electron quasimomenta and contains only the exchange splitting. Of course, at $E_{SOC}/E_{ex0} \gtrsim 1$ our NIMR mechanism quantitatively modifies, which requires further investigation. However, in the studied compound EuSn₂As₂ the exchange splitting $E_{ex0} \approx 30 \text{meV}$, while the spin-orbit coupling $E_{SOC} \lesssim 5 \,\mathrm{meV} \ll E_{ex0}$, as follows from our DFT calculations (see **Supplementary Note 4**). Hence, we can safely neglect the SOC.

The influence of the redistribution of spin-density of conduction electrons on the exchange interaction between the Eu atoms is also ignored. This redistribution may only slightly affect the RKKY interaction between the Eu atoms. The redistribution of spin density of conduction electrons by AFM order is small by parameter $\gamma \ll 1$, while their charge density remains practically unchanged. Moreover, the main contribution to the exchange interaction between the Eu atoms comes from the direct exchange and superexchange coupling via intermediate localized electrons of Sn and As orbitals rather than from the RKKY mechanism. This can be estimated directly or

concluded from the weak dependence of the AFM coupling on the electron density tuned by pressure [31] in $EuSn_2As_2$ or by doping in a sister compound $EuIn_2As_2$ [33].

Our ARPES measurements and band structure calculations for bulk $\operatorname{EuSn_2As_2}$ [25] show no band crossings and Dirac points at the Fermi level (see Supplementary Note 4), and are consistent with calculations of Ref. [7]. The magnetotransport measurements also showed that $\delta R(H)/R(0)$ is almost independent of the field direction H||ab| or H||c, of the charge transport direction, in-plane $R_{ab}(H)$ or normal to the plane $R_c(H)$ (see Fig. 4 and Ref. [25]). NIMR is also independent of the angle between the electric and magnetic field in the easy ab-plane [25] (see **Supplementary Note 5**). These results exclude the axion insulator origin of NIMR in $\operatorname{EuSn_2As_2}$. The similarity of NIMR in various materials also indicates insignificance of the Dirac states close to E_F , such as in $\operatorname{EuSn_2P_2}$ [10].

Neither our, nor other ARPES measurements and DFT band structure calculations for EuSn_2As_2 [7, 25, 34] reveal Dirac cones at E_F . In addition, resistivity temperature dependence for EuSn_2As_2 in all works [8, 9, 25, 30] shows a monotonic decrease almost down to T_N , thus evidencing a conventional semimetalic-, rather than topological insulator-type behavior, such as suggested in Ref. [32]. These results provide solid ground for the applicability of our model to EuSn_2As_2 .

The independence of NIMR on the sample thickness (from 60 nm to 0.2 mm) [35] indicates that NIMR does not come from scattering by large-scale lattice defects (such as misfit dislocations, misoriented grains), and is irrelevant to the zero-field electron scattering rate $1/\tau_0$, since these parameters are to be different for various samples, for the bulk crystal and exfoliated flakes a few monolayer thick. Whereas the NIMR magnitude is about the same for all studied samples and for various field directions, its shape for some samples in low fields looks somewhat more flattened, that might be caused by a minor positive MR contribution due to magnon scattering [25]

The proposed magnetoresistance model is widely universal. The approximately parabolic and isotropic negative magnetoresistance measured in this work is similar to that observed earlier in EuSn₂As₂ [9, 31], and in sister materials – EuSn₂P₂ [10], CaCo₂As₂ [11], and CsCo₂Se₂ [12]. We, therefore, believe that our model is applicable to the listed layered AFM-ordered compounds. It may also be partially applicable to EuFe₂As₂, though the in-plane properties of this compound are affected by Fe-moments stripe ordering [22, 23], which causes anisotropy of NMR.

In order to illustrate the universality of the proposed mechanism, we show below the magnetoresistance $\delta R(H)$ data for several vdW layered compounds in the AFM state (i.e. at $T < T_N$) and compare them qualitatively with Eq. (12). In all cases, the MR data scale with field $H_{\rm sf}$ of magnetization saturation, where the $H_{\rm sf}$ value is taken from the magnetization measurements. As for the

magnitude of NIMR effect, since $(E_{ex0}/2t_0)$ -value is unavailable in the published papers, it was used as a adjusting parameter to fit $\Delta R(H)/R(0)$ at the point $H = H_{\rm sf}$. In all compounds this parameter takes reasonable values. One can see that the predicted parabolic dependence $\delta R(H)$ qualitatively fits the data; the deviation (e.g., on panel d) may be associated with oversimplified character of the lowest-order model that ignores, e.g., the positive MR from electron-magnon scattering (for discussion, see Ref. [25] and the references therein).

It is worth noting, the panel (f) for EuMg₂Bi₂ shows a more complex non-monotonic MR in a weak field $H \ll H_{\rm sf}$ in addition to the predicted NIMR effect. Nevertheless, the abrupt termination of NIMR at $H = H_{\rm sf}$ is firmly connected with the magnetization saturation, as well as in all listed above AFM layered semimetals, in agreement with our model. Concerning the low-field R(H) feature in EuMg₂Bi₂, we note firstly that the magnetoresistance rise in low field is observed for the in-plane transport with magnetic field also aligned in the basal plane. Secondly, the positive MR slowly broadens but does not decay with temperature increasing up to about [36] 100 K and, finally, it overpowers NIMR at T > 20 K. These two facts do not allow to associate the positive MR at $H \ll H_{\rm sf}$ with antilocalization. The EuMg₂Bi₂ material is considered to be the nodal-line semimetal with linear-dispersing bands at the Fermi level [36]. Since in this AFM-material the FM-type spin fluctuations have been found to dominate, the sign-changing MR was discussed in Ref. [36] in terms of the competition between the AFM and FM orders. Also, for EuMg₂Bi₂ the spinorbit coupling is found to be crucially essential for the band structure at the Fermi level and makes the topological invariant equal to 1; therefore, the influence of non-trivial topology on magnetotransport should be important. Obviously, complex magnetoresistance behavior in this interesting material requires detailed studies.

There are other even more complex behaviors of magnetoresistance in more complex layered materials, for example, in ferromagnetic Weyl semimetal EuCd₂As₂ [37], in axion insulator EuIn₂As₂ [2, 38], and AFM topological insulators EuMg₂Bi₂ [36], MnBi₂Te₄ and MnBi₄Te₇ [39, 40]. These cases are beyond the framework of suggested simple model, but even in these compounds our mechanism may considerably contribute to the observed negative magnetoresistance, e.g., as we see from Fig. 6f.

To conclude, we clarified the origin of the negative isotropic magnetoresistance observed in layered AFM semimetals. Specifically, we suggested a novel type of magnetoresistance mechanism and developed a theory describing NIMR over a wide field range up to complete spin polarization. In the proposed theory, the negative magnetoresistance originates from the violation of \hat{T}_2 symmetry and the corresponding stronger localization of electron wave functions on one of the two AFM sublattices depending on electron spin.

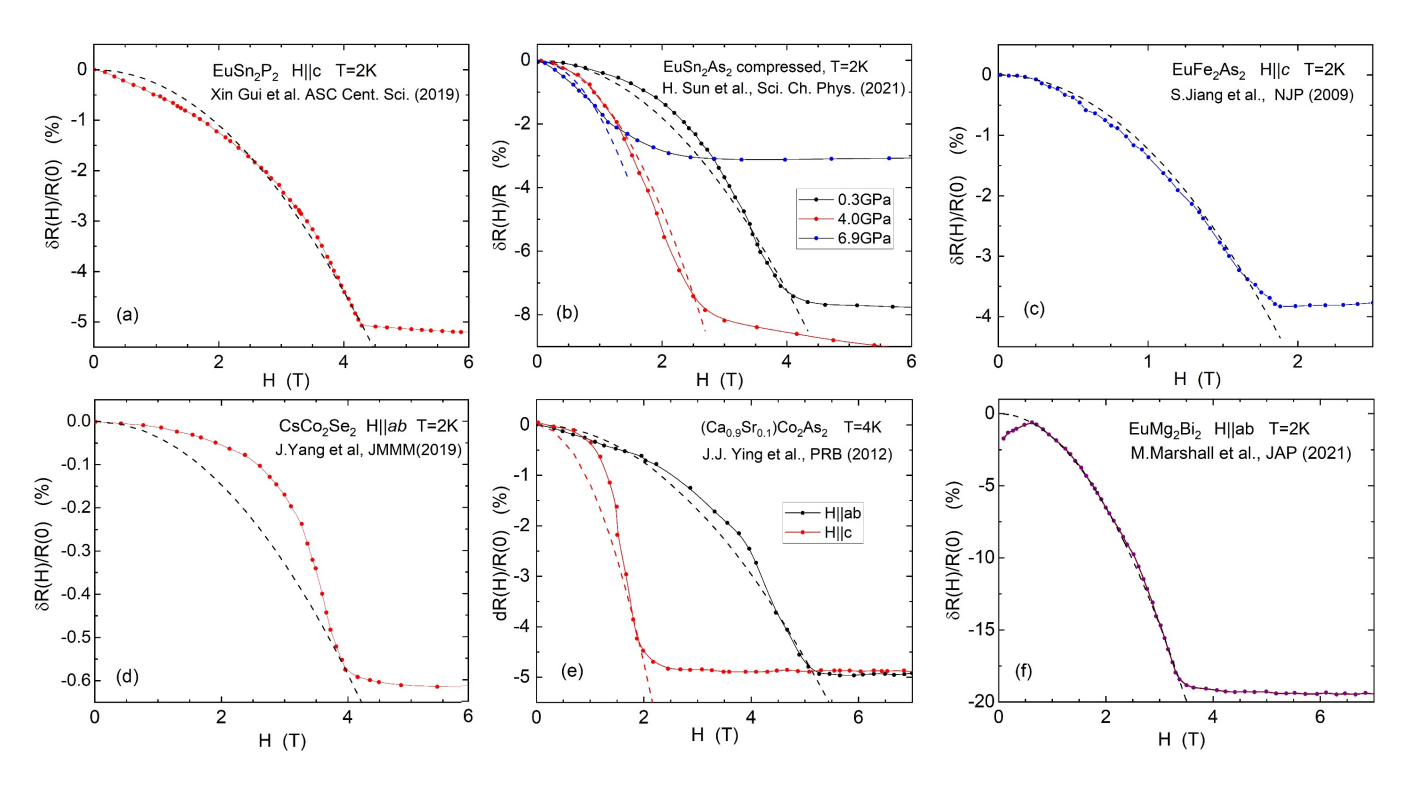


FIG. 6. Magnetoresistance $\delta R(H)/R(0)$ for several layered vdW materials in the AFM state. The experimental data are digitized from the published papers (symbols), and model curve are plotted according to Eq. (12) from the main text (dashed lines) for several compounds: (a) for EuSn₂P₂ from Fig. 5d of [10], (b) for the compressed EuSn₂As₂ from Ref. [31] at several pressure values indicated on the panel, (c) for EuFe₂As₂ from Fig. 6 of Ref. [22], (d) for CsCo₂Se₂ from Fig. 4 of Ref. [12], (e) for (CaSr)Co₂As₂ from Fig. 4 of Ref. [11], (f) for EuMg₂Bi₂ from Fig. 3 of Ref. [36].

The proposed mechanism of the parabolic NIMR is generic for the layered AFM semimetals; the NIMR magnitude is independent of the electron scattering rate and increases as the ratio of the exchange splitting to the transfer integral increases. The proposed model agrees qualitatively with the available data for layered AFM semimetals, such as EuSn₂As₂, EuSn₂P₂, EuFe₂As₂, CaCo₂As₂, CsCo₂Se₂, confirming negative isotropic magnetoresistance to be their intrinsic property, irrelevant to defects, domains, and other sample-specific disorder. Although the NIMR magnitude is about the same in all of the above compounds, $\approx 5-6\%$, their relevant energy spectrum parameters (E_{ex0} and t_0) are unknown, which prevents a detailed comparison with theory.

The proposed model of the NIMR effect helps to extract useful information about the electronic structure of AFM compounds. Indeed, according to Eq. (12), the NIMR magnitude gives the parameter $\gamma_0 = E_{ex0}/2t_0$, i.e. the ratio of exchange energy splitting to the hopping amplitude between AFM sublattices. The proposed NIMR effect opens a platform for the detection and study of magnetic ordering using electron transport measurements.

Methods

Experimental. The magnetotransport measurements were preformed with CFMS-16 cryomagnetic system, and

using standard 4-terminal AC technique with SR830 lock-in amplifier. Magnetization measurements were done with PPMS-7 SQUID magnetometer.

The EuSn₂As₂ single crystals were synthesized from homogeneous SnAs (99.99% Sn + 99.9999% As) precursor and elemental Eu (99.95%) in stoichiometric molar ratio (2:1) using the growth method, similar to our previous works [24, 41]. For magnetization measurements we selected bulk crystals of EuSn₂As₂, $\approx 1-2$ mm in the ab-plane and ≈ 0.1 mm thick; transport measurements were done both with same bulk crystals and with exfoliated flakes.

DFT calculations. The DFT band structure calculations were performed within the DFT+U approximation in the VASP software package [42]. The generalized gradient approximation (GGA) in the form of the Perdew-Burke-Ernzerhof (PBE) exchange-correlation functional [43] was employed. The onsite Coulomb interaction of Eu-4f electrons was described with the DFT+U scheme with the Dudarev approach [44] (U=5.0 eV same as in Ref. [32]).

Data availability The data that support the findings of this study are available from the corresponding author upon reasonable request.

- H. Li, H. He, H.-Z. Lu, H. Zhang, H. Liu, R. Ma, Z. Fan, S.-Q. Shen, and J. Wang, Negative magnetoresistance in Dirac semimetal Cd3As2, Nature Communications 7, 10301 (2016).
- [2] J. Yan, Z. Z. Jiang, R. C. Xiao, W. J. Lu, W. H. Song, X. B. Zhu, X. Luo, Y. P. Sun, and M. Yamashita, Fieldinduced topological Hall effect in antiferromagnetic axion insulator candidate EuIn₂As₂, Phys. Rev. Res. 4, 013163 (2022).
- [3] J. Li, C. Wang, Z. Zhang, B.-L. Gu, W. Duan, and Y. Xu, Magnetically controllable topological quantum phase transitions in the antiferromagnetic topological insulator MnBi₂Te₄, Phys. Rev. B 100, 121103 (2019).
- [4] J. Ge, Y. Liu, J. Li, H. Li, T. Luo, Y. Wu, Y. Xu, and J. Wang, High-Chern-number and high-temperature quantum Hall effect without Landau levels, National Science Review 7, 1280 (2020), https://academic.oup.com/nsr/article-pdf/7/8/1280/38881797/nwaa089.pdf.
- [5] J. Xiong, S. K. Kushwaha, T. Liang, J. W. Krizan, M. Hirschberger, W. Wang, R. J. Cava, and N. P. Ong, Evidence for the chiral anomaly in the Dirac semimetal Na3Bi, Science 350, 413 (2015), https://www.science.org/doi/pdf/10.1126/science.aac6089.
- [6] X. Huang, L. Zhao, Y. Long, P. Wang, D. Chen, Z. Yang, H. Liang, M. Xue, H. Weng, Z. Fang, X. Dai, and G. Chen, Observation of the Chiral-Anomaly-Induced Negative Magnetoresistance in 3D Weyl Semimetal TaAs, Phys. Rev. X 5, 031023 (2015).
- [7] M. Q. Arguilla, N. D. Cultrara, Z. J. Baum, S. Jiang, R. D. Ross, and J. E. Goldberger, EuSn2As2: an exfoliatable magnetic layered Zintl-Klemm phase, Inorg. Chem. Front. 4, 378 (2017).
- [8] H.-C. Chen, Z.-F. Lou, Y.-X. Zhou, Q. Chen, B.-J. Xu, S.-J. Chen, J.-H. Du, J.-H. Yang, H.-D. Wang, and M.-H. Fang, Negative Magnetoresistance in Antiferromagnetic Topological Insulator EuSn2As2, Chinese Physics Letters 37, 047201 (2020).
- [9] H. Li, W. Gao, Z. Chen, W. Chu, Y. Nie, S. Ma, Y. Han, M. Wu, T. Li, Q. Niu, W. Ning, X. Zhu, and M. Tian, Magnetic properties of the layered magnetic topological insulator EuSn₂As₂, Phys. Rev. B 104, 054435 (2021).
- [10] X. Gui, I. Pletikosic, H. Cao, H.-J. Tien, X. Xu, R. Zhong, G. Wang, T.-R. Chang, S. Jia, T. Valla, W. Xie, and R. J. Cava, A new magnetic topological quantum material candidate by design, ACS Central Science 5, 900 (2019).
- [11] J. J. Ying, Y. J. Yan, A. F. Wang, Z. J. Xiang, P. Cheng, G. J. Ye, and X. H. Chen, Metamagnetic transition in $\text{Ca}_{1-x}\text{Sr}_x\text{Co}_2\text{As}_2(x=0 \text{ and } 0.1)$ single crystals, Phys. Rev. B **85**, 214414 (2012).
- [12] J. Yang, W. Yang, Q. Zhu, B. Chen, H. Wang, Q. Mao, J. Du, Z. Lou, and M. Fang, Spin-flop transition and magnetic phase diagram in CsCo2Se2 revealed by torque and resistivity measurements, Journal of Magnetism and Magnetic Materials 474, 70 (2019).
- [13] M. B. Fontes, J. C. Trochez, B. Giordanengo, S. L. Bud'ko, D. R. Sanchez, E. M. Baggio-Saitovitch, and M. A. Continentino, Electron-magnon interaction in RNiBC (R = Er, Ho, Dy, Tb, and Gd) series of compounds based on magnetoresistance measurements, Phys.

- Rev. B **60**, 6781 (1999).
- [14] H. Yamada and S. Takada, Magnetoresistance of antiferromagnetic metals due to s-d interaction, Journal of the Physical Society of Japan 34, 51 (1973), https://doi.org/10.1143/JPSJ.34.51.
- [15] H. Yamada and S. Takada, Magnetoresistance due to electron-spin scattering in antiferromagnetic metals at low temperatures, Progress of Theoretical Physics 49, 1401 (1973), https://academic.oup.com/ptp/articlepdf/49/5/1401/5409531/49-5-1401.pdf.
- [16] We presume that for our case of the easy magnetization ab plane, the $\mathbf{H}||ab$ and $\mathbf{H}||c$ field orientations correspond, in notations of Ref. [15], to the easy axis $\mathbf{H}||z$, and perpendicular to it $\mathbf{H}||x$, respectively.
- [17] M. N. Baibich, J. M. Broto, A. Fert, F. N. Van Dau, F. Petroff, P. Etienne, G. Creuzet, A. Friederich, and J. Chazelas, Giant Magnetoresistance of (001)Fe/(001)Cr Magnetic Superlattices, Phys. Rev. Lett. 61, 2472 (1988).
- [18] E. Dagotto, T. Hotta, and A. Moreo, Colossal magnetoresistant materials: the key role of phase separation, Physics Reports 344, 1 (2001).
- [19] R. E. Camley and J. Barnas, Theory of giant magnetoresistance effects in magnetic layered structures with antiferromagnetic coupling, Phys. Rev. Lett. 63, 664 (1989).
- [20] A. Barthélémy, A. Fert, and F. Nguyen Van Dau, Giant magnetoresistance, in *Encyclopedia of Materials: Science* and *Technology*, edited by K. J. Buschow, R. W. Cahn, M. C. Flemings, B. Ilschner, E. J. Kramer, S. Mahajan, and P. Veyssière (Elsevier, Oxford, 2001) pp. 3521–3531.
- [21] W.-G. Yin and R. Tao, Effective-medium theory of the giant magnetoresistance in magnetic granular samples and doped LaMnO₃ perovskites, Phys. Rev. B 62, 550 (2000).
- [22] S. Jiang, Y. Luo, Z. Ren, Z. Zhu, C. Wang, X. Xu, Q. Tao, G. Cao, and Z. Xu, Metamagnetic transition in EuFe2As2 single crystals, New Journal of Physics 11, 025007 (2009).
- [23] J. J. Sanchez, G. Fabbris, Y. Choi, Y. Shi, P. Malinowski, S. Pandey, J. Liu, I. I. Mazin, J.-W. Kim, P. Ryan, and J.-H. Chu, Strongly anisotropic antiferromagnetic coupling in EuFe₂As₂ revealed by stress detwinning, Phys. Rev. B 104, 104413 (2021).
- [24] I. Golovchanskiy, E. Maltsev, I. Shchetinin, V. Vlasenko, P. Dzhumaev, K. Pervakov, O. Emelyanova, A. Tsvetkov, N. Abramov, V. Pudalov, and V. Stolyarov, Magnetic resonances in EuSn2As2 single crystal, Journal of Magnetism and Magnetic Materials 562, 169713 (2022).
- [25] K. S. Pervakov, A. V. Sadakov, O. A. Sobolevskiy, V. A. Vlasenko, V. P. Martovitsky, E. A. Sedov, E. I. Maltsev, N. Perez, L. Veyrat, P. D. Grigoriev, N. S. Pavlov, I. A. Nekrasov, O. E. Tereshchenko, V. A. Golyashov, and V. M. Pudalov, Intrinsic Negative Magnetoresistance in Layered AFM Semimetals: the Case of EuSn₂As₂ (2024), arXiv:2411.03971 [cond-mat.supr-con].
- [26] A. A. Abrikosov, Fundamentals of the theory of metals (North-Holland Sole distributors for the USA and Canada, Elsevier Science Pub. Co, Amsterdam New York, NY, USA, 1988).
- [27] V. S. Mandel', V. D. Voronkov, and D. E. Gromzin, Antiferromagnetic Resonance In MnO, Soviet Journal of Experimental and Theoretical Physics Letters 36, 521 (1973).
- [28] P. K. Streit and G. E. Everett, Antiferromagnetic reso-

- nance in EuTe, Phys. Rev. B 21, 169 (1980).
- [29] C. Kittel, Quantum theory of solids (Wiley, New York, 1963).
- [30] S. Pakhira, M. A. Tanatar, T. Heitmann, D. Vaknin, and D. C. Johnston, A-type antiferromagnetic order and magnetic phase diagram of the trigonal Eu spin-⁷/₂ triangularlattice compound EuSn₂As₂, Phys. Rev. B **104**, 174427 (2021).
- [31] H. Sun, C. Chen, Y. Hou, W. Wang, Y. Gong, M. Huo, L. Li, J. Yu, W. Cai, N. Liu, R. Wu, D.-X. Yao, and M. Wang, Magnetism variation of the compressed antiferromagnetic topological insulator EuSn2As2, Science China Physics, Mechanics & Astronomy 64, 118211 (2021).
- [32] H. Li, S.-Y. Gao, S.-F. Duan, Y.-F. Xu, K.-J. Zhu, S.-J. Tian, J.-C. Gao, W.-H. Fan, Z.-C. Rao, J.-R. Huang, J.-J. Li, D.-Y. Yan, Z.-T. Liu, W.-L. Liu, Y.-B. Huang, Y.-L. Li, Y. Liu, G.-B. Zhang, P. Zhang, T. Kondo, S. Shin, H.-C. Lei, Y.-G. Shi, W.-T. Zhang, H.-M. Weng, T. Qian, and H. Ding, Dirac Surface States in Intrinsic Magnetic Topological Insulators EuSn₂As₂ and MnBi_{2n}Te_{3n+1}, Phys. Rev. X 9, 041039 (2019).
- [33] J. Yan, J. Si, Z. Jiang, H. Ma, Y. Uwatoko, B.-T. Wang, X. Luo, Y. Sun, and M. Yamashita, Doping-tunable Fermi surface with persistent topological Hall effect in the axion candidate EuIn₂As₂, Phys. Rev. B 110, 115111 (2024).
- [34] X. Lv, X. Chen, B. Zhang, P. Jiang, and Z. Zhong, Thickness-Dependent Magnetism and Topological Properties of EuSn2As2, ACS Applied Electronic Materials 4, 3212 (2022).
- [35] E. I. Maltsev, L. Veyrat, N. R. Perez, R. Giraud, J. Dufouleur, B. Büchner, K. S. Pervakov, and V. M. Pudalov, Anomalous Hall Effect in EuSn₂As₂ Thin Flakes, To be published elsewhere.
- [36] M. Marshall, I. Pletikosić, M. Yahyavi, H.-J. Tien, T.-R. Chang, H. Cao, and W. Xie, Magnetic and electronic structures of antiferromagnetic topological material candidate EuMg2Bi2, Journal of Applied Physics 129, 035106 (2021).
- [37] S. Roychowdhury, M. Yao, K. Samanta, S. Bae, D. Chen, S. Ju, A. Raghavan, N. Kumar, P. Constantinou, S. N. Guin, N. C. Plumb, M. Romanelli, H. Borrmann, M. G. Vergniory, V. N. Strocov, V. Madhavan, C. Shekhar, and C. Felser, Anomalous Hall Conductivity and Nernst Effect of the Ideal Weyl Semimetallic Ferromagnet EuCd2As2, Advanced Science 10, 2207121 (2023).
- [38] F. H. Yu, H. M. Mu, W. Z. Zhuo, Z. Y. Wang, Z. F. Wang, J. J. Ying, and X. H. Chen, Elevating the magnetic exchange coupling in the compressed antiferromagnetic axion insulator candidate EuIn₂As₂, Phys. Rev. B 102, 180404 (2020).
- [39] J. Ge, Y. Liu, J. Li, H. Li, T. Luo, Y. Wu, Y. Xu, and J. Wang, High-Chern-number and high-temperature quantum Hall effect without Landau levels, National Science Review 7, 1280 (2020), https://academic.oup.com/nsr/articlepdf/7/8/1280/38881797/nwaa089.pdf.
- [40] A. Tan, V. Labracherie, N. Kunchur, A. U. B. Wolter,

- J. Cornejo, J. Dufouleur, B. Büchner, A. Isaeva, and R. Giraud, Metamagnetism of weakly coupled antiferromagnetic topological insulators, Phys. Rev. Lett. **124**, 197201 (2020).
- [41] Y. F. Eltsev, K. S. Pervakov, V. A. Vlasenko, S. Y. Gavrilkin, E. P. Khlybov, and V. M. Pudalov, Magnetic and transport properties of single crystals of Fe-based superconductors of 122 family, Phys. Usp. 57, 827 (2014).
- [42] G. Kresse and J. Furthmüller, Efficient iterative schemes for ab initio total-energy calculations using a plane-wave basis set, Phys. Rev. B 54, 11169 (1996).
- [43] J. P. Perdew, K. Burke, and M. Ernzerhof, Generalized gradient approximation made simple, Phys. Rev. Lett. 77, 3865 (1996).
- [44] S. L. Dudarev, G. A. Botton, S. Y. Savrasov, C. J. Humphreys, and A. P. Sutton, Electron-energy-loss spectra and the structural stability of nickel oxide: An LSDA+U study, Phys. Rev. B 57, 1505 (1998).

ACKNOWLEDGEMENTS

The authors thank V.N. Menshov for useful discussions. AVS, OAS, and VMP were supported within State Assignment of the research at LPI. PDG acknowledges State Assignment # FFWR-2024-0015. NSP, IAN and IRS acknowledge partial support of the State Assignment # 124022200005-2 of Institute of Electrophysics and # 124020600024-5 of Institute of Solid State Chemistry UB RAS. AVS, OAS, VMP, NSP and IAN acknowledge support from RSCF (grant # 23-12-00307). Experimental work was partly done using equipment of LPI Shared facility Center.

AUTHOR CONTRIBUTIONS

P.D.G. composed the theoretical model and performed analytical calculations, N.S.P., I.A.N., and I.R.S. performed numerical DFT calculations. K.S.P., and E.M., grew and characterized the bulk crystals, V.M.P., A.V.S., and O.A.S. planned and designed the experiments, analyzed and processed the data. A.V.S., and O.A.S. performed magnetization and magnetotransport measurements with bulk samples. E.M. prepared the flake samples, E.M. performed measurements with flakes and processed their results. P.D.G. and V.M.P. wrote the paper with considerable help from all authors. All the authors contributed to the discussion of the experimental results.

ADDITIONAL INFORMATION

The paper contains supplementary material.

Correspondence and requests for materials should be addressed to Pavel D. Grigoriev at grigorev@itp.ac.ru.

Supplementary Information for

Universal negative magnetoresistance in antiferromagnetic metals caused by symmetry breaking of electron wave functions

Pavel D. Grigoriev*, 1, 2, 3 Nikita S. Pavlov, 4, 5 Igor A. Nekrasov, 4 Ilya R. Shein, 6 Andray V. Sadakov, 5 Oleg A. Sobolevskiy, 5 Evgeny Maltsev, 7, 8 and Vladimir M. Pudalov 1 L.D. Landau Institute of Theoretical Physics, RAS

2 National University of Science and Technology "MISiS", 119049, Moscow, Russia

3 HSE University, Moscow 101000, Russia

4 Institute for Electrophysics, RAS, Ekaterinburg, 620016, Russia

5 V. L. Ginzburg Research Center at P. N. Lebedev Physical Institute, RAS, Moscow 119991, Russia

6 Institute of Solid State Chemistry, RAS, Ekaterinburg, 620990, Russia

7 Leibniz Institute for Solid State and Materials Research, IFW Dresden, D-01069 Dresden, Germany

8 Dresden-Würzburg Cluster of Excellence ct.qmat, Dresden, Germany

*Correspondence to: grigorev@itp.ac.ru

CONTENTS

I.	Supplementary	Note 1:	Magnetization field dependence	2
II.	Supplementary	Note 2:	On the Topology of ESA Band Structure	3
III.	Supplementary	Note 3:	Alignment of the Eu Magnetic Moments in ESA	4
IV.	Supplementary	Note 4:	Influence of spin-orbit coupling to the band structure	5
V.	Supplementary	Note 5:	On the Isotropy of the Negative Magnetoresistance in ESA	6
	References			7

I. SUPPLEMENTARY NOTE 1: MAGNETIZATION FIELD DEPENDENCE

Our DC-magnetization measurements have been performed earlier with single crystal samples from the same batch [1]. Figure S1 shows results of magnetization measurements with EuSn₂As₂ (ESA) sample [1] in two orientations of the sample in magnetic field. For the proposed magnetoresistance model, it is essential only that as field increases, M(H) curves (at the lowest temperatures) demonstrate a sharp saturation of the magnetization. The saturation field values are taken as complete spin polarization field $H_{\rm sf}$. For different field orientations these values are different: $H_{\rm sf} = 3.6\,\mathrm{T}$ when magnetic field is applied in the ab planes and $H_{\rm sf} = 4.9\,\mathrm{T}$ when magnetic field is applied along the c- axis. In the field range $H \leq H_{\rm sf}$, magnetization M develops linearly with field, thus substantiating our derivation of Eq. (10) of the main paper. The M(T) curves (Figure S1c) [1] show the magnetic transition at temperature $T_N \approx 24\,\mathrm{K}$, manifested by the kink, which corresponds to the antiferromagnetic spin ordering in the Eu sub-lattice of ESA. Both, the saturation fields and the critical temperature, are well consistent with values reported for ESA compound previously [2–4].

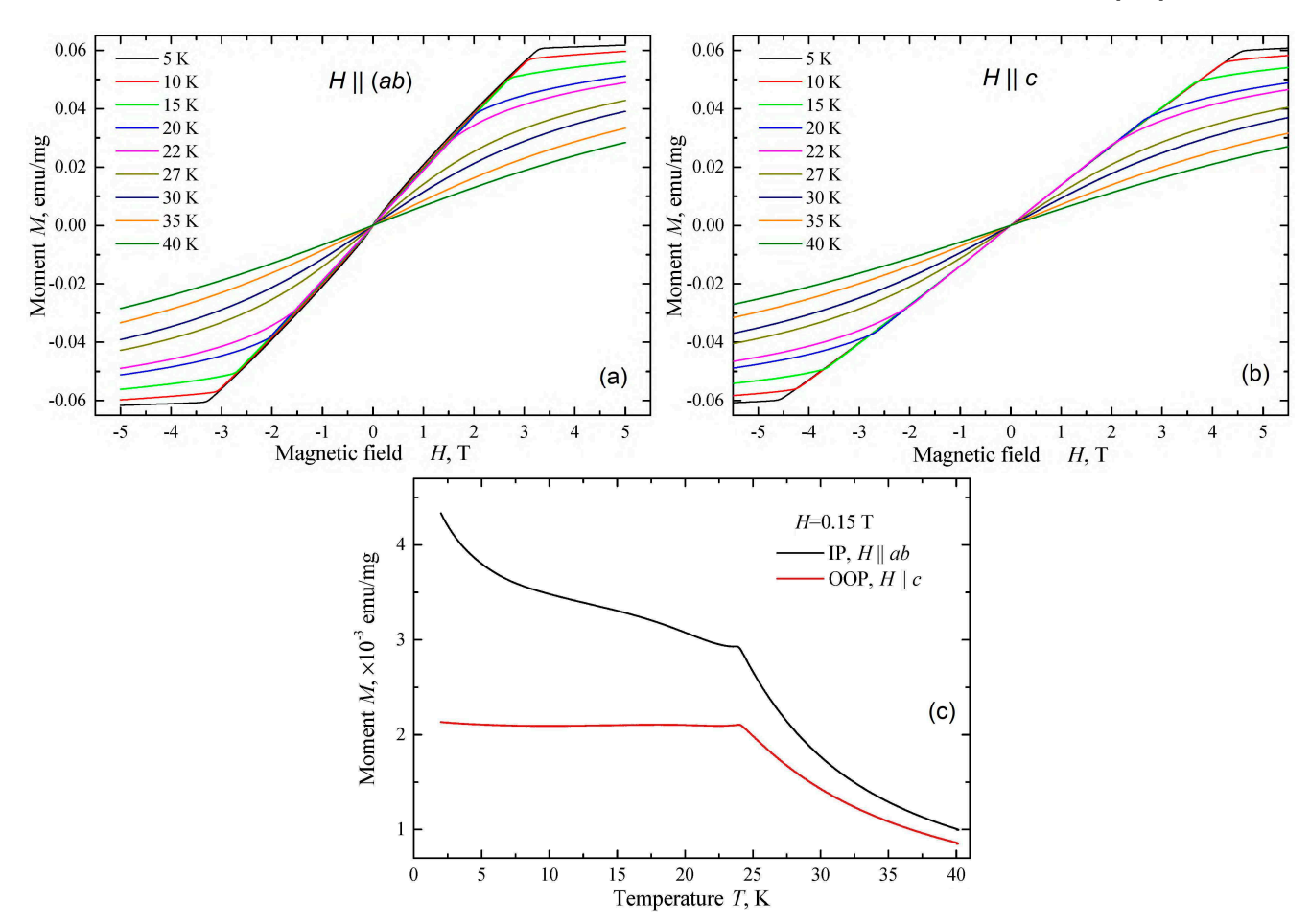


Fig. S1 | Magnetization dependence on magnetic field and temperature for EuSn₂As₂ single crystal M(H) at several fixed temperatures for magnetic field applied: a, in-plane (IP, along the ab crystal plane), and b, out-of-plane (OOP, along the c crystal direction). (c) Temperature dependence of magnetization M(T) measured with DC field H = 0.15 T for the two orientations of magnetic field. Adapted from Ref. [1].

II. SUPPLEMENTARY NOTE 2: ON THE TOPOLOGY OF ESA BAND STRUCTURE

From the band structure (BS) calculations, Arguilla et al. [5] found Dirac points in the spectrum, essentially above E_F . In subsequent calculations, Li et al. [2] has suggested EuSn₂As₂ to be either a strong topological insulator (TI) or axion insulator (AI) [2, 6].

On the experimental side, the first possibility (TI) is inconsistent with the observations as follows:

- (i) monotonic temperature dependence of the zero field resistivity. $\rho(T)$ decreases smoothly with cooling both in-plane ρ_{ab} and out of plane ρ_c , in the antiferromagnetic and paramagnetic states (except for a minor kink at T_N [3, 6, 7] in the vicinity of the AFM transition, related with magnetic fluctuations). In other words, no signs of surface states (SS) conduction is found in transport;
- (ii) ARPES measurements and calculations of the electron band structure don't reveal Dirac points, gap, and SS in the close vicinity of the Fermi level.

Thus, the experimental results indicate a semimetallic, rather than insulator nature of the ESA compound with no gap at E_F .

Regarding the existence of the AI state: for testing this interesting possibility we measured the anisotropy of magnetoresistance in the AFM state (for more detail, see Supplementary Note 4). Regarding the potential TI phase and the existence of SS states, we note that by time-resolved ARPES measurements [2] the Dirac crossing point was found to lie $0.4\,\mathrm{eV}$ above E_F and therefore may not affect charge transport at low temperatures. The absence of Dirac point and of the protected surface states in the vicinity of E_F was also confirmed by ARPES measurements in Ref. [7].

III. SUPPLEMENTARY NOTE 3: ALIGNMENT OF THE EU MAGNETIC MOMENTS IN ESA

The type of magnetic ordering in the AFM state of layered vdW semimetals with magnetic ions (such as $EuSn_2As_2$, $EuFe_2As_2$, $EuSn_2P_2$, $EuMg_2Bi_2$, $EuMg_2Sb_2$, etc.) was debatable in literature several years ago. There is general agreement in the scientific community that the Eu 4f magnetic moments in $EuSn_2As_2$ and in other sister compounds form an A-type structure in the AFM state. By definition, the A-type structure means that the ab planes are ferromagnetic and couple antiferromagnetically along the c axis. However, whether the ferromagnetic moments are directed along the c-axis (the "easy axis" configuration), or aligned in the ab-plane ("easy-plane" configuration) was initially a subject of discussions, which we briefly review below.

In the BS calculations [2] for ESA it was not determined which of the two configurations, AFM-b, or AFM-c has lower energy (and, hence, is realized in practice). In Figure 1 of Ref. [2], the Eu magnetic moments are drawn along the c axis, though we stress that no evidence for such choice was presented in Ref. [2]. Later on, Pakhira et al. [4] reported neutron diffraction measurements which also confirmed the Eu moments are ferromagnetically aligned in the ab plane, lie in the ab plane, and are stacked antiferromagnetically along the c axis. Strictly speaking, the in-plane direction of the FM moments cannot be determined from neutron diffraction alone. For the sister compound, EuFe₂As₂, from additional symmetry analysis of magnetic reflections data in neutron diffraction studies [8] and from magnetic resonant x-ray scattering [10] it was concluded that Eu²⁺ moments lie in the (ab)-plane. Similar conclusion was drawn for EuMg₂Bi₂ [9] by using additionally the Bilbao crystallographic server [11].

This seemingly controversial issue, nevertheless, may be easily resolved using common sence arguments and simple molecular field theory as follows:

- (i) For an isolated layer of Eu atoms with the moments aligned ferromagnetically in-plane, the *ab*-plane alignment is more energetically favorable than *c*-axis alignment by $\Delta E = 0.29 \,\mathrm{meV}$; this corresponds to a magnetic field anisotropy $H_{\rm anis} = \Delta E/(7\mu_B) = 7.25 \,\mathrm{kOe}$ [4].
- (ii)For the bulk ESA crystal, the measured DC-magnetization M(H) curves (see Fig. S1 and also Refs. [1, 3–5]) clearly indicate the saturation field $H_{\rm sf}$ larger for $H\|c$ than for $H\perp c$ field direction. This is because the free energy in the magnetic sublattice expression contains a positive magnetic anisotropy term K_U which makes the Eu-spins direction $\|(ab)$ preferable (see Eq. (1) of Ref. [1]). Consequently, the saturation fields for in-plane and out-of-plane orientations are different: $H_{\rm sf}^{ab} = 2H_e = 2J/M_s$ and $H_{\rm sf}^c = 2J/M_s + M_s + 2K_U/M_s$, where J is the exchange constant, H_e is the exchange field, and M_s the saturation magnetization. From the measured magnetization curves (Figs. S1a,b) at $T \ll T_N$ we find $K_U = 1.4 \times 10^5 \text{J/m}^3$, the term that ensures the in-plane Eu-spins alignment in the AFM state at zero field.
- (iii) Temperature dependence of the AC magnetic susceptibility measured in weak fields for H||c direction remains almost constant below $T = T_N$ at a value $\chi(T) \approx \chi(T = T_N)$. In contrast, for $H \perp c$ it drops by a factor of two (see Fig. 8 of Ref. [4]). This is well consistent with the simple mean field theory calculations [12, 13], **namely for magnetic moments lying in the** (ab) **plane** (see [4] and discussion therein). It is worth noting, such measurements, to be conclusive, should be done in very low fields (≤ 100 Gs) and the results are often distorted by the presence of ferromagnetic impurities and ferromagnetic-type defects in the sample.

Finally, we note that the debatable issue of the Eu moments direction in ESA at zero magnetic field, along the c-axis, or along the (ab)-plane, is insignificant for the proposed model of NIMR that is applicable for both cases, and is isotropic. Indeed, since σ in Eqs. (5) and (6) denotes the spin projection on the AFM order parameter L_{AFM} , these and all subsequent formulas remain valid for any direction of L_{AFM} .

IV. SUPPLEMENTARY NOTE 4: INFLUENCE OF SPIN-ORBIT COUPLING TO THE BAND STRUCTURE

The band structure calculated with spin-orbit coupling (SOC) (red lines) is shown in Figure S2. There aren't pronounced split bands due to the SOC. General influence of SOC is manifested in the bands shifting. Looking closely, we can see a small splitting of the bands near the Fermi level around Γ -point (insert in the Figure S2) that has a magnitude about 5 meV. This splitting is missing in case of the SOC absence (blue lines), therefore we associate it with the spin-orbit interaction. In addition, away of the Fermi energy, there are areas where the distance between bands has increased in case of SOC included, these are visible as small shifts of about 5–10 meV. Hence we conclude, the spin-orbit interaction energy can be estimated no larger than 10 meV everywhere and ≤ 5 meV in the vicinity of E_F .

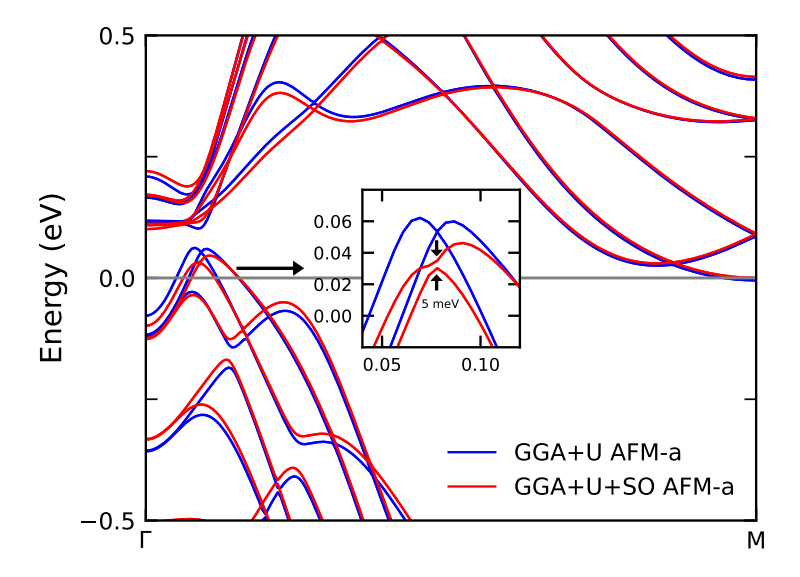


Fig. S2 | The comparison of GGA+U band structure with (red) and without (blue) spin-orbit interaction in the non-collinear regime (AFM-a).

V. SUPPLEMENTARY NOTE 5: ON THE ISOTROPY OF THE NEGATIVE MAGNETORESISTANCE IN ESA

In the band structure calculations for ESA, Li et al. [2] considered two possible configurations: AFM-b, and AFM-c. It was concluded (i) the PM state in ESA is a strong topological insulator (STI) but "with no observable gap inside", (ii) the AFM-b state in ESA is an axion insulator (AI) and topological crystalline insulator with surface states crossing at E_F , and (iii) the AFM-c phase is AI with gapped SS.

In order to verify the possibility of the predicted AI state, we measured anisotropy of the in-plane magnetoresistance at $T \ll T_N$ by varying the magnetic field **H** direction relative to the bias current **J** direction. Figure S3 shows that the negative magnetoresistance is practically isotropic, within the experimental errors. This isotropy does not support the possibility of the axion insulator state which is known to be highly anisotropic.

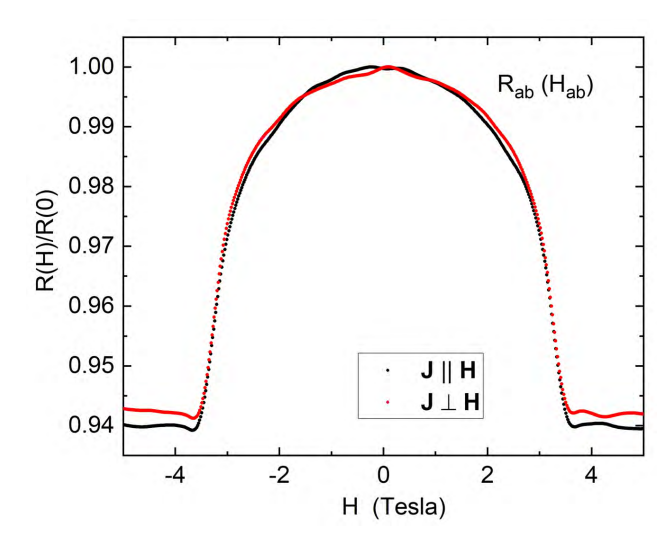


Fig. S3 | In-plane magnetoresistance R(H)/R(H=0) measured with EuSn₂As₂ single crystal for magnetic field lying in the ab-plane, and for two orientations of the field H relative to the bias current J.

Supplementary references

- I. A. Golovchanskiy, E. I. Maltsev, I. V. Shchetinin, V. A. Vlasenko, P. S. Dzhumaev, K. S. Pervakov, O. V. Emelyanova, A. Yu. Tsvetkov, N. N. Abramov, V. M. Pudalov, V. S. Stolyarov, Magnetic resonances in EuSn₂As₂ single crystal, *J. Magn. Magn. Mater.*, **562**, 169713 (2022)
- [2] Hang Li et al. Dirac Surface States in Intrinsic Magnetic Topological Insulators EuSn_2As_2 and $\text{MnBi}_{2n}\text{Te}_{3n+1}$. Phys. Rev. X 9, 041039 (2019).
- [3] Huan-Cheng Chen, Zhe-Feng Lou, Yu-Xing Zhou, Qin Chen, Bin-Jie Xu, Shui-Jin Chen, Jian-Hua Du, Jin-Hu Yang, Hang-Dong Wang, and Ming-Hu Fang, Negative Magnetoresistance in Antiferromagnetic Topological Insulator EuSn₂As₂, *Chin. Phys. Lett.* **37**, No. 4, 047201 (2020).
- [4] S. Pakhira, M. A. Tanatar, T. Heitmann, D. Vaknin, and D. C. Johnston, A-type antiferromagnetic order and magnetic phase diagram of the trigonal Eu spin-7/2 triangular-lattice compound EuSn₂As₂. *Phys. Rev. B* **104**, 174427 (2021).
- [5] M. Q. Arguilla, N. D. Cultrara, Z. J. Baum, S. Jiang, R. D. Ross and J. E. Goldberger et al. EuSn₂As₂: an exfoliatable magnetic layered Zintl-Klemm phase *Inorg. Chem. Front.* 4, 378 (2017).
- [6] H. Li, W. Gao, Z. Chen et al. Magnetic properties of the layered magnetic topological insulator EuSn₂As₂, Phys. Rev. B 104, 054435 (2021).
- [7] K. S. Pervakov, A. V. Sadakov, O. A. Sobolevskiy, V. A. Vlasenko, V. P. Martovitsky, E. I. Maltsev, N. Pérez, L. Veyrat, P. D. Grigoriev, N. S. Pavlov, I. A. Nekrasov, O. E. Tereshchenko, V. A. Golyashov, and V. M. Pudalov, Intrisic Negative Magnetoresistance in Layered AFM Semimetals: the Case of EuSn₂As₂. https://arxiv.org/abs/2411.03971
- [8] Y. Xiao, Y. Su, M. Meven, R. Mittal, C. M. N. Kumar, T. Chatterji, S. Price, J. Persson, N. Kumar, S. K. Dhar, A. Thamizhavel, and Th. Brueckel, Magnetic structure of EuFe₂As₂ determined by single-crystal neutron diffraction, Phys. Rev. B 80, 174424 (2009)
- [9] S. Pakhira, F. Islam, E. O'Leary, M. A. Tanatar, T. Heitmann, R. Prozorov, A. Kaminski, D. Vaknin, and D. C. Johnston,A-type antiferromagnetic order in semiconducting EuMg2Sb2 single crystals, Phys. Rev. B 106, 024418 (2022)
- [10] J. Herrero-Mart?n, V. Scagnoli, C. Mazzoli, Y. Su, R. Mittal, Y. Xiao, T. Brueckel, N. Kumar, S. K. Dhar, A. Thamizhavel, and L. Paolasini, Magnetic structure of EuFe2As2 as determined by resonant X-ray scattering, Phys. Ref. B 80, 134411 (2009).
- [11] J. M. Perez-Mato, S. V. Gallego, E. S. Tasci, L. Elcoro, G. de la Flor, and M. I. Aroyo, Symmetry-Based Computational Tools for Magnetic Crystallography, Annu. Rev. Mater. Res. 45, 217 (2015).
- [12] D. C. Johnston, Magnetic Susceptibility of Collinear and Noncollinear Heisenberg Antiferromagnets, Phys. Rev. Lett. 109, 077201 (2012).
- [13] D. C. Johnston, Unified molecular field theory for collinear and noncollinear Heisenberg antiferromagnets, Phys. Rev. B 91, 064427 (2015).